Quasiparticle energy bands of transition-metal oxides within a model *GW* scheme

S. Massidda
Istituto Nazionale di Fisica della Materia-Dipartimento di Scienze Fisiche, Università degli Studi di Cagliari, I-09124 Cagliari, Italy

A. Continenza
Istituto Nazionale di Fisica della Materia-Dipartimento di Fisica, Università degli Studi dell'Aquila, I-67010 Coppito, L'Aquila, Italy

M. Posternak* and A. Baldereschi*
Institut de Physique Appliquée, Ecole Polytechnique Fédérale, PHB Ecublens, CH-1015 Lausanne, Switzerland
(Received 15 October 1996)

We calculate the quasiparticle band structure of NiO and $CaCuO_2$ by using a model self-energy correction which approximates closely the *GW* method of Hedin. We obtain energy gaps and magnetic moments in agreement with experiment. For NiO, our results agree with integrated and angle-resolved photoemission experiments in the low binding energy region. The spectral distributions of O $2p$ and Ni $3d$ states are discussed, in relationship with the available experimental data. Our results demonstrate that the addition of self-energy corrections to local-spin-density band calculations provides a meaningful description of many aspects of the electronic states of transition-metal oxides. As expected, the satellite structures observed in photoemission experiments are not found in our calculations. [S0163-1829(97)00619-X]

I. INTRODUCTION

The interest in the electronic structure of the late transition-metal monoxides (TMO's) MnO, FeO, CoO, and NiO (Ref. 1) has been revived by the discovery of the high-temperature superconductors, since TMO's share with the parent compounds of the latter an antiferromagnetic insulating behavior, related to the large value of the on-site $3d$ Coulomb repulsion energy U. The local-spin-density (LSD) band calculations are unable to describe the localized nature of these electron states, and lead to very tiny magnetic moments and small or vanishing band gaps. Furthermore, there is a discrepancy between the calculated and observed spectral weights for metal $3d$ and O $2p$, as well as for their relative energy locations. On the basis of the above problems associated with the LSD band-structure picture, and because of the success of the localized configuration-interaction (CI) cluster method[2,3] in describing the electronic states of TMO's, it has often been argued that the former approach should be ruled out for these materials.

Recent photoemission[4–6] (PES) and inverse-photoemission[6,7] experiments in NiO have shown that both the localized and the itinerant pictures have some relevance in the description of TMO's. In particular, the dispersion of the O $2p$ bands is well described by the LSD calculations. Furthermore, very recent PES results[8] suggest that the first ionization states, usually interpreted in terms of $d^8 \rightarrow d^8\underline{L}$ ($\underline{L}$ meaning oxygen ligand hole) excitations display also a large k-vector dispersion, not very different from that obtained by LSD calculations. However, significant discrepancies remain between LSD results and experimental data. Since limitations in identifying the Kohn-Sham eigenvalues as excitation energies of the many-electron system are well known, these discrepancies are not surprising but call for more sophisticated calculations. Alternative approaches such as the self-interaction corrected density functional theory[9–11] and the model LSD+U method[12] have been used, to cure the LSD pathologies, leading to significant improvements in the values of magnetic moments and energy gaps. Among the works based on the above methods, however, only the one by Arai and Fujiwara[11] provide quasiparticle band structures, which can be compared to the available detailed angle-resolved photoemission results.

A succesful method for calculating quasiparticle excitation energies in semiconductors is the *GW* approximation,[13] which represents the lowest order of many-body perturbation theory in terms of the fully screened electron-electron interaction, and gives the electron self-energy Σ^{GW} as the product of the interacting Green's function G times the dynamically screened Coulomb potential W. Despite its obvious interest, however, computational difficulties have prevented until recently its use in TMO's. This is especially true considering that (apart from some recent all-electron approaches[14,15]) most of the implementations of the *GW* approximation are based on the plane-wave pseudopotential method,[16–18] not easily applicable to TMO's. Only recently, Aryasetiawan and Gunnarsson[19] have calculated the *GW* band structure of NiO, based on the linear muffin-tin orbital method and with some approximation in the self-consistency.

Recently, we calculated[20] the electronic structure of MnO, using a (self-consistent) model derived from the method proposed by Gygi and Baldereschi,[21] which reproduces accurately the results of a complete *GW* calculation with a much reduced computational effort. An encouraging agreement was found with experiment, in terms of energy gap, magnetic moment, bandwidth, and spectral distribution of Mn $3d$ states. The weak satellite observed at high binding energy (BE), however, was not found, which is not surprising since our self-energy corrections are energy independent. In this paper, we report a similar self-consistent calculation of the electronic structure of NiO and $CaCuO_2$. We find a good agreement with experiment in terms of magnetic moments

and band gaps. Furthermore, in NiO, the energy location of TM d bands, relative to the O $2p$ bands, as well as their spreading over several eV, is corrected relative to LSD and is in substantial agreement with angle-integrated photoemission and O $K\alpha$ x-ray emission data. We also obtain a good agreement with the most recent angle-resolved photoemission data for NiO, in the low BE region. As in the case of MnO, however, our calculations do not provide the high BE satellites observed in photoemission experiments. Comparison of self-consistent and non-self-consistent results stresses the need to include self-consistently self-energy corrections in transition-metal oxides, due to large changes in the electronic wave functions. Our results show therefore that our model GW scheme is able to give a reasonable description of the electronic states of these systems, improving significantly upon LSD.

The paper is organized as follows: in Sec. II we describe the method; test applications to simple semiconductors are reported in Sec. III. In Sec. IV we describe the results for NiO and $CaCuO_2$ and, finally, in Sec. V we draw our conclusions.

II. METHOD

In the GW approximation, the electron self-energy is given by

$$\Sigma^{GW}(\mathbf{r},\mathbf{r}';E)=\frac{i}{2\pi}\int G(\mathbf{r},\mathbf{r}';E+E')W(\mathbf{r},\mathbf{r}';E')dE', \tag{1}$$

where G is the full interacting Green's function, and W is the dynamically screened Coulomb interaction. The latter is described by the dielectric matrix ε^{-1},

$$W(\mathbf{r},\mathbf{r}';E)=\int d\mathbf{r}''\varepsilon^{-1}(\mathbf{r},\mathbf{r}'';E)v(\mathbf{r}''-\mathbf{r}'), \tag{2}$$

where v is the bare Coulomb interaction. In the approximated method introduced by Gygi and Baldereschi,[21] one separates the self-energy into a short-range and a long-range term. The short-range term can be approximated by the Kohn-Sham local exchange-correlation potential, while the long-range term takes into account the incomplete screening of the Coulomb interaction in nonmetals, and decays fairly rapidly in reciprocal space. We start by writing the self-energy as

$$\Sigma^{GW}(\mathbf{r},\mathbf{r}';E)=\frac{i}{2\pi}\int G(\mathbf{r},\mathbf{r}';E+E')W^{\mathrm{IEG}}(\mathbf{r},\mathbf{r}';E')dE' + \frac{i}{2\pi}\int G(\mathbf{r},\mathbf{r}';E+E')\delta W(\mathbf{r},\mathbf{r}';E')dE', \tag{3}$$

where W^{IEG} is the short-range effective potential of a metallic inhomogeneous electron gas. Following Sham and Kohn,[22] the corresponding self-energy contribution, which depends only on the density in the vicinity of $\mathbf{r}$ and $\mathbf{r}'$ ($|\mathbf{r}-\mathbf{r}'|\leq\max\{\lambda_F,\lambda_{\mathrm{TF}}\}$, where λ_F and λ_{TF} are the Fermi and Thomas-Fermi screening lengths, respectively) can be approximated by a local exchange-correlation potential [in our case, the Kohn-Sham energy-independent $\mu_{\mathrm{xc}}(\mathbf{r})$].

The second term of Eq. (3) [referred to as $\delta\Sigma$ in the following, and formally defined through Eqs. (1) and (3)], is nonlocal and should contain the contribution from the long-range part of the Coulomb interaction, incompletely screened in semiconductors and insulators. It is known that in nonmetals δW behaves asymptotically at large separation as $1/(\varepsilon_\infty|\mathbf{r}-\mathbf{r}'|)$ (where ε_∞ is the static electronic dielectric constant), and that the screening properties at short separation are the same for all materials with a given density. We may now simplify further the problem by assuming that $\delta W(\mathbf{r},\mathbf{r}';E)$ depends only on $|\mathbf{r}-\mathbf{r}'|$, i.e., neglecting local-field and dynamical corrections. Indeed, calculations have shown that local-field effects become negligible when $|\mathbf{r}-\mathbf{r}'|$ is larger than the interatomic distance. Also, the energy dependence of $\delta\Sigma$ is assumed to be dominated by a plasmon-pole structure around the plasmon frequency ω_p, which is much higher than the energy excitations considered. We note, however, that the approximation of neglecting local fields and dynamical effects is not done on the whole self-energy, but only on $\delta\Sigma$. Performing the energy integrations in the second term of Eq. (3), we obtain

$$\delta\Sigma(\mathbf{r},\mathbf{r}')=-\rho(\mathbf{r},\mathbf{r}')\delta W(|\mathbf{r}-\mathbf{r}'|), \tag{4}$$

where $\rho(\mathbf{r},\mathbf{r}')$ is the one-body density matrix. We write the Fourier transform of δW as

$$\delta W(\mathbf{q})=\frac{4\pi e^2}{\Omega q^2}[\varepsilon_{\mathrm{SC}}^{-1}(\mathbf{q};\omega=0)-\varepsilon_M^{-1}(\mathbf{q};\omega=0)], \tag{5}$$

where $\varepsilon_{\mathrm{SC}}^{-1}$ and ε_M^{-1} represent the diagonal response of a semiconductor and of a metal, respectively. Our experience for Si has shown that the term in square brackets in Eq. (5), written $\delta\varepsilon^{-1}(q)$, is a smooth function of $\mathbf{q}$ which dies off at around $q_{\mathrm{cut}}\approx 2$ a.u.[21] Since, in general, we do not know the detailed shape of $\delta\varepsilon^{-1}(q)$, we used in the present work two different models. The simplest one is a step function $\delta\varepsilon^{-1}(q)=(1/\varepsilon_\infty)\theta(q_{\mathrm{cut}}-q)$, where q_{cut} is a cutoff parameter related to the Fermi or to the Thomas-Fermi screening length, and the static electronic dielectric constant ε_∞ is taken from experiment. While for simple sp semiconductors the results depend very marginally on this cutoff, a relatively larger dependence is found in TMO's. Tests performed for MnO and NiO as a function of q_{cut} showed that, in the range $2<q_{\mathrm{cut}}<4$ a.u., the results are sufficiently stable, with a small increase ($\approx 0.03\mu_B$) of the magnetic moment and eigenvalue differences changing by ≈ 0.2 eV. We use $q_{\mathrm{cut}}=3$ a.u. in the following. In the second model we write $\delta\varepsilon^{-1}(q)=\varepsilon_{LL}^{-1}(q)-\varepsilon_L^{-1}(q)$, where $\varepsilon_{LL}^{-1}(q)$ and $\varepsilon_L^{-1}(q)$ are the inverse diagonal parts of the Levine-Louie[23] model and the Lindhard dielectric functions, respectively. The two models share the limit $\delta\varepsilon^{-1}(0)=1/\varepsilon_\infty$, but in the intermediate q region they differ significantly, with the second model going down to zero at ≈ 3 a.u. Despite these differences between the models, the largest changes in the total bandwidth and in the band gap of NiO were at most ≈ 0.4 eV, which we consider to be the limit of accuracy of our model GW calculations. In the following, we report the results obtained with the step function model for $\delta\varepsilon^{-1}(q)$.

$\delta\Sigma$ is diagonalized in the basis of the LSD Bloch functions, as discussed in Ref. 24. We have

$$(\hat{H}^{\mathrm{LDA}}+\delta\Sigma)\psi_{n\mathbf{k}}=\epsilon_{n\mathbf{k}}\psi_{n\mathbf{k}}, \tag{6}$$

$$\psi_{n\mathbf{k}}=\sum_{n'} z_{nn'}\psi^{\mathrm{LDA}}_{n'\mathbf{k}}, \tag{7}$$

and we expand the electronic Bloch functions in terms of the accurate full-potential linearized-augmented-plane-wave basis set.[25] We are then lead to the following secular equation:

$$\|(\epsilon^{\mathrm{LDA}}_{n\mathbf{k}}-\epsilon_{n\mathbf{k}})\delta_{nn'}+\langle n'\mathbf{k}|\delta\Sigma|n\mathbf{k}\rangle\|=0, \tag{8}$$

which gives us the corrected quasiparticle eigenstates. In semiconductors the off-diagonal matrix elements of $\delta\Sigma$ are quite small, which implies that first-order perturbative corrections to the eigenvalues are already sufficient. When dealing with NiO or $CaCuO_2$, however, we need to carry out the procedure self-consistently. Several iterations (≈ 12) are needed in order to converge, starting from the LSD ground state. Around ten empty states are sufficient to lead to converged valence states. In order to calculate the matrix elements in Eq. (8), we introduce the ''overlap charge densities'' defined by

$$\rho_{m\mathbf{q},n\mathbf{k}}(\mathbf{r})=\psi^{*}_{m\mathbf{q}}(\mathbf{r})\psi_{n\mathbf{k}}(\mathbf{r}), \tag{9}$$

and the corresponding Fourier transforms

$$\rho_{m\mathbf{q},n\mathbf{k}}(\mathbf{G}_j)=\int_I \rho_{m\mathbf{q},n\mathbf{k}}(\mathbf{r})\exp[-i(\mathbf{k}-\mathbf{q}+\mathbf{G}_j)\cdot\mathbf{r}]d\mathbf{r} + \sum_{\alpha}\int_{S_\alpha}\rho_{m\mathbf{q},n\mathbf{k}}(\mathbf{r})\exp[-i(\mathbf{k}-\mathbf{q}+\mathbf{G}_j)\cdot\mathbf{r}]d\mathbf{r}, \tag{10}$$

where the integrals with labels I and S_α are performed over the interstitial region and muffin-tin spheres, respectively, and α runs over the atoms in the unit cell. We may write the matrix elements of $\delta\Sigma$ as

$$\langle n'\mathbf{k}|\delta\Sigma|n\mathbf{k}\rangle=-4\pi e^2\sum_{j,\mathbf{q}}\delta\varepsilon^{-1}(|\mathbf{k}-\mathbf{q}+\mathbf{G}_j|) \times\sum_{m}^{\mathrm{occ}}\frac{\rho^{*}_{m\mathbf{q},n'\mathbf{k}}(\mathbf{G}_j)\rho_{m\mathbf{q},n\mathbf{k}}(\mathbf{G}_j)}{|\mathbf{k}-\mathbf{q}+\mathbf{G}_j|^2}. \tag{11}$$

These matrix elements are formally similar to those obtained within the Hartree-Fock or diagonally screened exchange schemes, apart from the presence of $\delta\varepsilon^{-1}$ which reduces the computational load. In fact, since our step model for $\delta\varepsilon^{-1}$ cuts off at quite low momenta (≈ 3 a.u.), it is straightforward to perform the **G**-vector summation in Eq. (11). This makes the present approach computationally much faster, and easier to implement than the Hartree-Fock or, even worse, the full GW method. The singularity found in Eq. (11) for $\mathbf{k}\rightarrow\mathbf{q}$ and $\mathbf{G}_j=\mathbf{0}$ is treated as explained in Ref. 24; further technical details may be found in the same paper.

TABLE I. LDA, model GW, full GW, and experimental band gaps and the average energy of d states relative to the VBM (E_g and E_d, respectively) for some selected semiconductors (in eV).

Compound	LSD	Present work	GW	Expt.
		E_g (eV)		
Si	0.5	1.1	1.3,[a] 1.24,[b] 1.0,[c] 1.2[d]	1.2[e]
C	4.0	5.8	5.6,[a] 5.3,[b] 7.2,[d] 5.7[f]	5.5[e]
CdS	0.89	2.60	2.45[g]	2.50, 2.55[h]
ZnO	0.93	4.23[i]		3.44[i]
		E_d (eV)		
CdS	−7.6	−8.4	−8.1[g]	−9.5[j]
ZnO	−5.4	−6.4[i]		−8.6, −7.5[k]

[a]From Ref. 16.
[b]From Ref. 17.
[c]From Ref. 14.
[d]From Ref. 18.
[e]From Ref. 26.
[f]From Ref. 27.
[g]From Ref. 28.
[h]From Ref. 29.
[i]From Ref. 33.
[j]From Refs. 30 and 31.
[k]From Ref. 32.

III. RESULTS FOR SEMICONDUCTORS

Before examining the transition-metal oxides, we compare in Table I our results for a few simple semiconductors with the corresponding available GW values and experimental[21,26–33] data. We can see that an agreement within ≈ 0.2 eV is found for sp semiconductors, both with full GW calculations, and with experiment. More interesting, however, is the comparison for the materials containing semicore d states, as ZnO and CdS. In these compounds the d bands are found between anion s and p bands, contributing to both the electronic and structural properties. Their BE is badly underestimated by the local-density approximation (LDA), while the Hartree-Fock method overestimates it by several eV.[32,33] The model GW approximation pushes these states down by ≈ 1 eV, but their BE is still underestimated by ≈ 1 eV. This may be due to effects beyond GW. These results may be relevant in the discussion (see below) on the relative location of d and p states in TMO's, although d states are much more localized in the ZnO and CdS cases. Our model GW calculations for CdS agree with the results of Rohlfing, Krüger, and Pollmann *et al.*,[28] in particular, with those obtained including the whole $n=4$ shell (n principal quantum number) in the valence states. In our case, core states are treated as in conventional all-electron LDA calculations, and including them in our self-energy correction would not make sense, since we are correcting the long-range (in real-space) part of the electron-electron interaction, well beyond the size of Cd 4s and 4p core states. The agreement with full GW results is within 0.15 eV for the gap, and within 0.3 eV for the d states energy location. We should point out here that the agreement of our results with full GW may come partially from a cancellation between local fields and dynamical effects, which was also found by Hy-

TABLE II. LSD, model GW, LSD+U, SIC, and experimental magnetic moments (in μ_B) and energy band gaps (in eV) for the systems investigated. The values in parentheses include the orbital contribution.

Compound	LSD	Present work	LDA+U[a]	SIC[b]	Expt.
		Magnetic moments (μ_B)			
MnO	4.29	4.52 (4.52)	4.61	4.49 (4.49)	4.79,[c] 4.58[d–g]
NiO	1.12	1.56 (1.83)	1.59	1.53 (1.80)	1.77,[c] 1.64,[h] 1.90[d]
$CaCuO_2$		0.42	0.66		0.51[i]
		Energy gaps (eV)			
MnO	1.0	4.2	3.5	3.98	3.8−4.2[j,k]
NiO	0.3	3.7	3.1	2.54	4.3,[l] 4.0[m]
$CaCuO_2$	0.0	1.4	2.1		1.5[n]

[a]From Ref. 12.
[b]From Refs. 9 and 10.
[c]From Ref. 35.
[d]From Ref. 36.
[e]From Ref. 37.
[f]From Ref. 38.
[g]From Ref. 39.
[h]From Ref. 41.
[i]From Ref. 34.
[j]From Ref. 42.
[k]From Ref. 43.
[l]From Ref. 2.
[m]From Ref. 40.
[n]From Ref. 44.

bertsen and Louie[16] when going from diagonal Coulomb-hole–screened-exchange (COHSEX) to full GW.

IV. RESULTS FOR TRANSITION-METAL OXIDES

A. Structural details

Calculations for NiO have been performed, assuming a magnetic cell of rhombohedral structure with space group D_{3d}^5 ($R\bar{3}m$). The lattice parameter corresponds to that of the paramagnetic NaCl structure with the observed lattice constant 4.195 Å . The atomic sphere radii for Ni, and O are 2.1, and 1.8 a.u., respectively. The crystallographic structure of $CaCuO_2$ is simple tetragonal with one formula unit per cell and space group D_{4h}^1 (P_4/mmm). The present calculations have been performed in the antiferromagnetic (AFM) magnetic double cell, with a body-centered tetragonal structure and space group D_{4h}^{17} (I_4/mmm). We use the experimental $Ca_{0.84}Sr_{0.16}CuO_2$ lattice constants $a=5.46$ Å and $c=6.4$ Å. Both the in-plane and the out-of-plane-spin arrangements were assumed to be antiferromagnetic.[34]

B. Band gaps and magnetic moments

The values of magnetic moments and energy gaps are summarized in Table II, and compared with both the experimental data[2,9,12,34–44] and the theoretical values obtained within the self-interaction corrected (SIC) density functional theory[9,10] and the LSD+U method.[12] For completeness, we also report in Table II the corresponding results for MnO.[20] The magnetic moments, corrected to take into account the orbital contribution,[45] are shown in parentheses. Our results are in good agreement with experiment and with the corresponding values obtained using the SIC (Refs. 9 and 10) and the LSD+U[12] methods, improving drammatically upon the LSD. In particular, our approach is in better agreement with experiment than both the SIC and LSD+U for almost all the energy gap values. A further discussion and comparison with the other theoretical schemes will be made on the basis of the densities of states.

C. NiO

Our previous model GW study of MnO (Ref. 20) gave quite satisfactory results. The present results for NiO are of great interest since (i) more detailed angle-resolved photoemission experiments are available, (ii) its electronic structure is more complex than that of MnO. Indeed, while Mn has a complete spin up $3d$ shell, Ni has a d^8 configuration in the NiO ground state, with the down spin e_g states empty and all the other d states full. As a consequence of this electronic configuration, LSD gives already a semiconducting gap, but this gap is much too small. In Fig. 1 we plot the model GW energy bands of NiO along the X-Γ-Z directions of the antiferromagnetic Brillouin zone, together with the LSD results. The bands with a strong dispersion located below -3.5 eV are mostly due to O $2p$ states, while the Ni $3d$ orbitals are responsible for the bands closer to the gap. To be more specific, the symmetry of some relevant states at the Z point is indicated in Fig. 1 by the symbols t_{2g} and e_g, with $\uparrow$ and $\downarrow$ indicating the states which are mostly localized on the Ni(1) and Ni(2) sublattices, respectively.[46] Very remarkably, in our model GW calculations, there is no gap between the O $2p$ and Ni $3d$ bands, which merge in a wide region around Γ, in contrast with the LSD results. Apart from this major difference, and from a change in the backfolded band around -5 eV (which gets more Ni $3d$ orbital character and becomes slightly more flat along Γ-Z), the overall shape of the O $2p$ bands is pretty similar in the model GW and within the LSD. By inspection of the wave functions we can identify the extrema of the O $2p$ complex at the Γ point as the lowest state at -6.9 eV and the twofold degenerate states at ≈ -1.7 eV.

One of the major differences between the LSD calculations and experiments consists in the orbital character of the first electron removal state, mostly Ni $3d$ in LSD, and mostly O in experiments. A general picture of the electronic states can be obtained from the total and partial densities of states (PDOS) (shown in Fig. 2) as calculated in the model GW scheme and in the LSD approximation. We can see the large

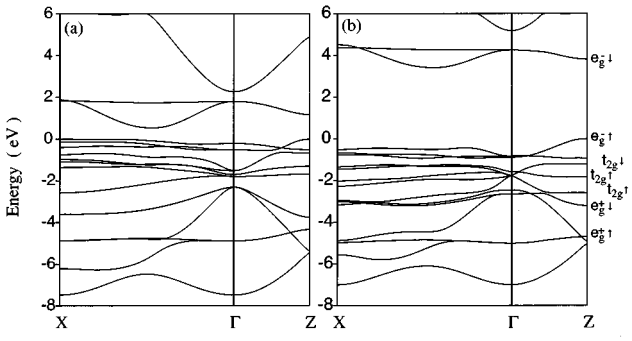

FIG. 1. LSD band structure (a) of NiO, along with the self-consistent model *GW* results (b).

(≈ 1 eV) shift of the Ni states towards the O bands, relative to the LSD case, which is in agreement with integrated photoemission[40] and O $K\alpha$ x-ray emission spectroscopy (XES) data.[47] However, the most striking correction is the spreading of the Ni character over the whole occupied energy range, and the enhanced O $2p$ character at the valence band maximum (VBM). Significantly, this shift of O and $3d$ weights (relative to LSD) is larger in NiO than in MnO,[20] which has a simpler electronic structure and which is considered to be of mixed charge-transfer Mott-Hubbard character. If we analyze, in particular, the orbital character of the e_g states, we find a large shift of the Ni $3d$ weight to higher BE, going from LSD to the model *GW*. In fact, the flat back-folded ''oxygen'' band at ≈ -5 eV is σ bonding with 60% Ni(1) and 29% O character at the Z point [37% Ni(1) and 50% O in LSD]. The corresponding e_g state at the Z-point VBM is σ antibonding with 36% Ni(1) and 55% O [59% Ni(1) and 35% O in LSD]. This character of VBM states is a mean-field analog of the first ionization state expected by many-body theory ($d^8\underline{L}$ states with E_g symmetry), and agrees with the predictions of LSD+U calculations of Anisimov, Zaanen, and Andersen.[12] The gap is found between these valence states having a substantial O component, and conduction states localized on the Ni(2) atoms [75% Ni(2) and 19% O], confirming the charge-transfer character of the gap in NiO. We notice that the energy distance between the above band at -5 eV and the center of gravity of Ni $3d$ conduction states is $\simeq 9$ eV, which is of the order of U.

In order to investigate further the differences between the LSD and the model *GW* results, we compare in Fig. 3 the total charge density calculated within the two schemes. The charge depletion on Ni sites, and the corresponding increase of the density around oxygen show that self-energy corrections enhance the ionic character of the compound. This results from the increased Ni contribution to e_g conduction states (the e_g character is evident in Fig. 3). This difference, however, is weak. If we integrate over the Ni muffin-tin spheres, we obtain $\approx 0.04e$ less in the model *GW* calculation than in the LSD case (per atom). This charge depletion is compensated by an equivalent gain inside O spheres.

The poles of one-electron Green's functions are directly related to the electron removal and addition energies, which are measured in direct and inverse-photoemission experiments. Although we are not really calculating the energy-dependent Green's function, it is of interest to compare our energy bands with the results of angle-resolved photoemission experiments (ARPES).[4,5] We report in Fig. 4 our bands, together with the published results of Refs. 4 and 5 in Figs. 4(a) and 4(b), respectively. The alignment between experimental and theoretical results is arbitrarily chosen in order to fit the highest valence state at Γ. Our results are in general good agreement with those of Shen *et al.*[4] in the low BE region. At Γ, in particular, all of the experimental points for $E > -3.5$ eV (the energy zero is chosen to be the VBM) correspond to calculated bands. Only the data points by Kuhlenbeck *et al.* at the lowest BE (in the middle of the Γ-

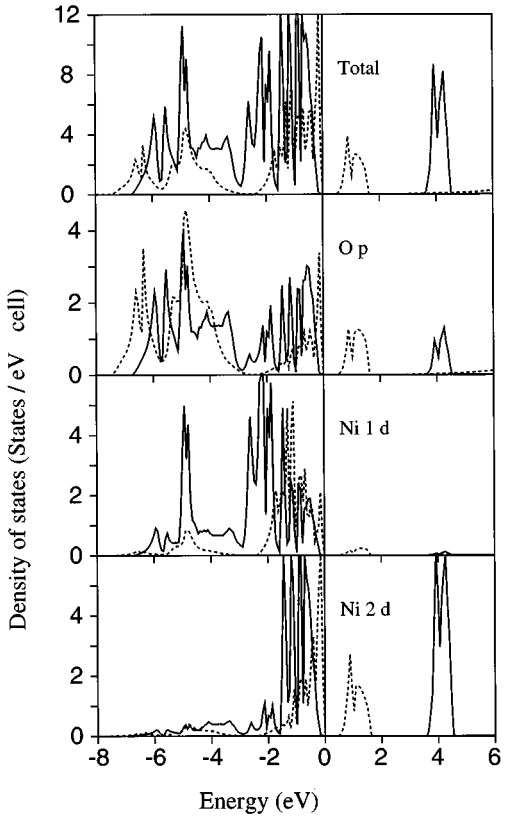

FIG. 2. Model *GW* (full lines) and the LSD (dashed lines) total and partial densities of states for NiO.

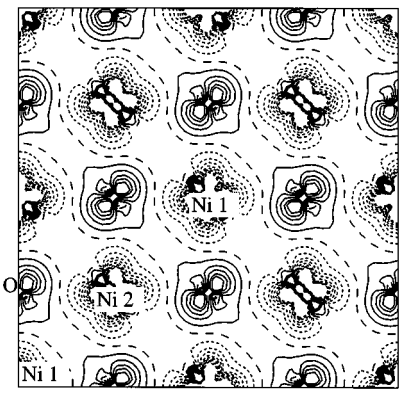

FIG. 3. Contour plots of the difference between the model *GW* and the LSD charge densities of NiO, along a (001) plane of the fcc cell. Full and short-dashed lines correspond to positive and negative contours, respectively, while the long-dashed lines correspond to the zero level. Levels are given in units of $10^{-3}e$/a.u.

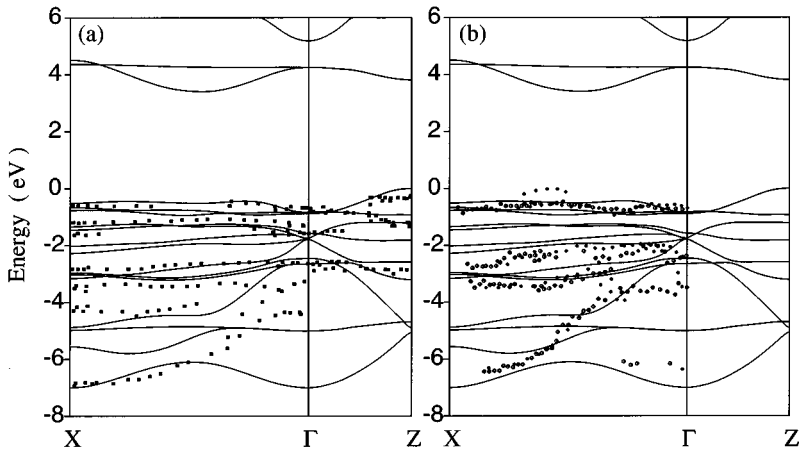

FIG. 4. Model GW self-consistent band structure of NiO, compared to the ARPES experiments by Shen *et al.* (Ref. 4) (a) and with those of Kuhlenbeck *et al.* (Ref. 5) (b). Experimental data along the Γ-Z line in (a) are by Shih (Ref. 8).

X line) are out of place, perhaps indicating a misalignment of experimental and theoretical results. In any event, a few improvements relative to the LSD can be noticed: (i) due to the increased dispersion along Γ-Z of the band at the VBM in the model GW, the highest valence band along the Γ-X line lies around 0.5 eV below the Fermi level, in closer agreement with the results of Shen *et al.*;[4] (ii) the energy location and dispersion of the bands in the range -3 to -3.5 eV at X, fits quite well the ARPES data, contrary to the LSD.

Considering the Ni $3d$ region, the most recent experimental angle-resolved photoemission data are those by Shih[8] along Γ-Z. This direction is well suited for a detailed band analysis, because of its high symmetry. The agreement between calculated and experimental ARPES data in Fig. 4 along this line is very good. All the experimental points coincide with bands calculated within the model GW scheme, and contrary to the LSD case,[8] this agreement extends down to Ni $3d$ states with higher binding energy (≈ -3 eV relative to the VBM). A particular but important aspect of this agreement concerns the dispersion of the e_g band, located at ≈ -1.7 eV at Γ and at the VBM at the Z point, after an anticrossing with the $t_{2g\downarrow}$ bands. This agreement is very important since it is the first time that ARPES experiments do show a significant dispersion for the first ionization states of NiO.

More problematic, however, is the comparison in the O $2p$ region. Although the dispersion of these bands is well reproduced by the calculations, the ARPES results of Shen *et al.*[4] seem to indicate higher BE. This is slightly less pronounced in the data by Kuhlenbeck *et al.*[5] The relative location of Ni $3d$ and O $2p$ bands is a controversial issue. Angle-integrated photoemission[40] and O $K\alpha$ XES (Ref. 47) experiments point to the necessity of a downward shift of LSD $3d$ bands by $\approx$ 2 eV, in agreement with our finding, and in apparent contrast with the indications of ARPES.

Since it may be relevant in this contest, we show in Fig. 5 the model GW energy bands, as obtained with the step model for $\delta\varepsilon^{-1}(q)$, and with the use of the Levine and Louie[23] dielectric function. The two sets of bands are very similar in the low BE region, and differ mostly in the gap, and in the distance between the O $2p$ and the Ni $3d$ states, which are, respectively, smaller and larger by a few tenths of an eV in the Levine and Louie model. This latter model seems to be in slightly better agreement with angle-resolved photoemission data.

In order to investigate further the problem of the O $2p$ vs Ni $3d$ relative energy location, we show in Fig. 6 the O $2p$ partial density of states obtained with a 0.5 eV Gaussian broadening. The model GW results have been shifted down by 0.7 eV in order to align perfectly the tails of the high BE O region. Due to atomiclike selection rules, these results should be comparable with the O $K\alpha$ XES data.[47] Relative to photoemission, XES has the advantage of being more bulk sensitive. The XES spectrum shows two major peaks, corresponding to the O band at higher BE, and to the Ni bands at lower BE. We can see that the model GW results agree much better with the XES measurements, both in terms of the relative energy location of peaks, and in terms of an increased O weight in the low BE region. The agreement regarding the shape of the O structure, however, is deteriorated in the model GW results, relative to LSD. This is mostly due to the changes occurring for the e_g states around -5 eV. Dynamical effects not taken into account by our model are probably necessary to improve the agreement with XES in this energy region.

Experimentally, the photoemission spectrum of NiO displays a high-energy satellite at about 9 eV below the Fermi level, usually interpreted as Ni d^7 final state excitations.[2,48] This peak, separated by an energy $U_{\rm eff}$ from the conduction band (Ni d^9 final states), corresponds in the CI language to a process in which an essentially unscreened $3d$ hole is created

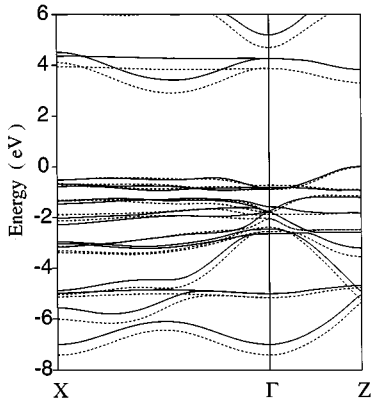

FIG. 5. Model GW self-consistent energy bands, obtained using a step function for $\delta\varepsilon^{-1}(q)$ (full lines), compared to those obtained using the Levine-Louie model (dashed lines).

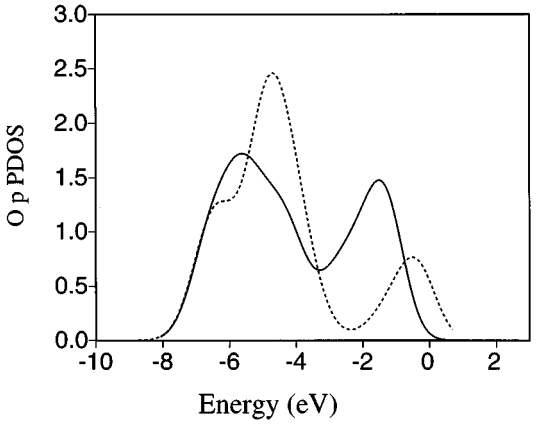

FIG. 6. O $2p$ partial density of states, broadened with a 0.5 eV Gaussian, obtained from model GW (full line) and LSD (dashed line).

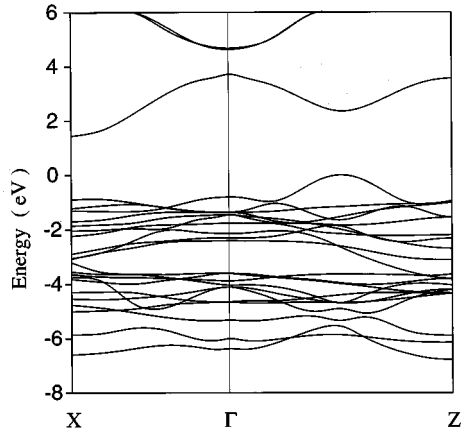

FIG. 7. Model GW energy bands of $CaCuO_2$ along the main symmetry lines of the AFM Brillouin zone.

on a metal atom, at the cost of a large energy.[49] In the CI approach the U_{eff} value is increased relative to the on-site interaction U by ligand-metal hybridization. The lower BE ionization states, on the other hand, correspond to $d^8 \rightarrow d^8\underline{L}$ excitations, describing the creation of a hole in the Ni $\underline{d}$ shell, followed by its screening by excitations involving the bandlike O states. The satellite is not found in our calculation; this discrepancy, which constitutes the major difference between our quasiparticle and the experimental electron removal spectra in NiO, is not surprising, since our model self-energy is energy independent. Furthermore, as pointed out by Aryasetiawan and Gunnarsson,[19] even the full GW approximation includes only in a mean-field way the creation of virtual electron-hole pairs (leading to the screening of the bare Coulomb interaction), but leaves out, e.g., ladder diagrams representing repeated hole-hole scatterings, which are expected to give rise to a strongly energy-dependent self-energy contribution. Therefore, we can expect the absence of a high BE satellite also in full GW calculations. Work is in progress in this direction, beyond the GW approximation.[50–53]

Considering the region $E > -8$ eV, it is very difficult to estimate what would be the effect of including such corrections. We can speculate, however, that the formation of a satellite would remove spectral weight from the states having large Ni character, namely, the states near the Fermi level, and the flat e_g bands at ≈ -5 eV, clearly identified in the Ni(1) PDOS. We can expect the related energy changes to be larger for the higher BE states, and to correspond very likely to an upward shift of the flat band at ≈ -5 eV. Such a shift would bring this band into better agreement with the photoemission experiments by Shen *et al.*,[4] in particular with the band indicated by crosses by these authors in their Fig. 12. The corresponding changes in the O p PDOS (an increased O content in the higher BE states) are also expected to improve the agreement with XES experiments. This view seems to be supported in the self-energy calculations by Manghi, Calandra, and Ossicini[50] and by Mizokawa and Fujimori.[53]

Finally, it is interesting to compare our results with the PDOS obtained by LSD+U (Ref. 12) and SIC (Ref. 10) calculations. Our PDOS show differences, but also important similarities with respect to the LSD+U calculations. As in our case, there is a large increase of O character in the low BE region relative to the LSD. This O component is larger in the LSD+U results (note, however, that we used different sphere radii). Another important similarity is the energy difference between the mostly $3d$ valence $e_g\uparrow$ states (the structure which is at $\simeq -5$ eV in our results) and the $3d$ $e_g\downarrow$ conduction band, which is at $\simeq 9$ eV. SIC-LSD results,[10,11] on the other hand, give most of the Ni $3d$ spectral weight below the O $2p$ bands. The ability of these calculations to reproduce correctly the low binding energy spectrum of NiO cannot be fully assessed from the present literature, and the relative main-line vs satellite intensity does not agree with the experimental situation. Basically, the same physics results from the Hartree-Fock method,[54] which gives the Ni $3d$ bands below the O $2p$ bands.

Since we are using a model GW approach we need to compare our results with the GW calculations by Aryasetiawan and Gunnarsson.[19] Given the tremendous effort required by a full GW calculation on a complex system, their calculation was not fully self-consistent, and cannot be directly compared with ours. Therefore, we performed a non-self-consistent model GW calculation (including nondiagonal matrix elements), using the self-consistent LSD potential and wave functions. Relative to the LSD bands, we found a large opening of the gap (≈ 2 eV), and a downward shift of $3d$ states; these bands, however, are quite different from the self-consistent ones. This is expected, since unlike the case of simple semiconductors, GW and LSD wave functions are significantly different from each other in an AFM system. Our results are in reasonable agreement with the bands of Ref. 19 (much more than the fully self-consistent model GW results of Fig. 1). In particular, we agree on the downward shift of the t_{2g} bands around -2 eV, and on the increased splitting of the two e_g-like states around -4 eV at Z. Considering the differencies between the two methods, we feel that this agreement is satisfactory.

D. $CaCuO_2$

We show in Fig. 7 the energy bands of $CaCuO_2$ along the X-Γ-Z lines of the AFM body-centered tetragonal Brillouin

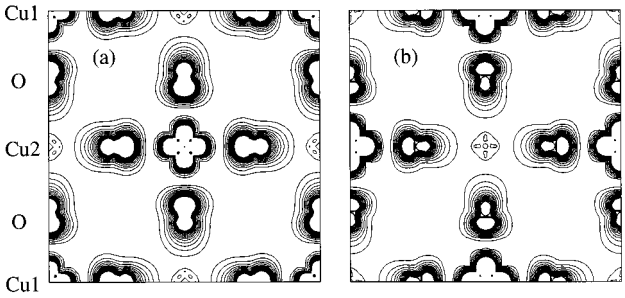

FIG. 8. Charge densities in the (001) plane corresponding to the states at the VBM (a) and CBM (b) at the Γ-Z midpoint.

zone. The situation for this compound differs from that of transition-metal monoxides, since the Cu $3d$ and O $2p$ states form here a single, strongly hybridized, $\simeq 7$ eV wide valence band. The conduction band is separated from the VBM at the Γ-Z midpoint by a gap of 1.4 eV [experiment gives 1.5 eV (Ref. 44)]. There is more symmetry in the band structure around the energy gap in $CaCuO_2$ than in TMO (see, for instance, Fig. 1). Due to the number of bands and to the complexity of their dispersion, we comment only on the highest occupied and lowest empty states, by plotting their charge distribution (calculated at the Γ-Z midpoint) in Fig. 8. We can see that these states are both $dp\sigma$ antibonding combinations of Cu $3d$ and O $2p$ orbitals, located on the two different spin sublattices. However, the VBM has a larger O character [28% Cu(1) and 55% O] relative to the conduction band minimum [50% Cu(2) and 37% O], evidencing the charge-transfer character of the gap. In Fig. 9 we plot the total and partial densities of states of $CaCuO_2$. As it is well known, the strongest chemical bonds in the high-temperature superconducting copper oxides are the in-plane Cu $d_{x^2-y^2}$ $-$O $p_{x,y}$ σ bonds. Therefore, we separate in Fig. 9 the partial density of π-bonded and of σ-bonded O p states, and we plot only the $d_{x^2-y^2}$ PDOS for the two Cu atomic sites. We see clearly that Cu(2) $d_{x^2-y^2}$ states contribute mostly to the conduction band, and that Cu(1) $d_{x^2-y^2}$ states are shared between the VBM region and the high BE structure at $\simeq -6$ eV. The energy separation between the conduction (down-spin) $d_{x^2-y^2}$ and these latter states is of the order of 8 eV, which agrees with the estimate of U for Cu $3d$ electrons. Our PDOS agree well with those given by the LSD$+U$ approach for $CaCuO_2$;[12] The latter calculations give an energy

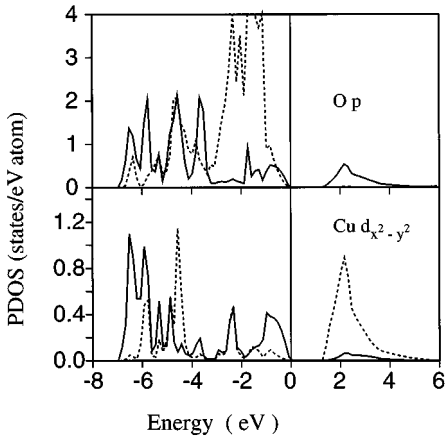

FIG. 9. Model GW total and partial densities of states for $CaCuO_2$. Full and dashed lines refer to σ and π-bonded O $2p$ states in the middle panel and to Cu(1) and Cu(2) σ-bonded $d_{x^2-y^2}$ states in the lower panel.

separation of $\simeq 8$ eV between the occupied spin $\uparrow$ and empty spin $\downarrow$ $d_{x^2-y^2}$ states, and the general shape of their PDOS and ours is very similar.

V. CONCLUSIONS

In summary, we have seen that our calculations, based on a model GW scheme, provide in many respects a reasonably good description of band gaps, magnetic moments, and of the low BE electron removal spectrum in TMO's, confirming tests of the method performed on simple semiconductors. The satellite structures observed in photoemission spectra, however, are not found in our calculations. Our results for NiO and $CaCuO_2$ are consistent with those of mean-field LSD$+U$ calculations.

ACKNOWLEDGMENTS

We thank J. Redinger for stimulating discussions and M. Grioni for constructive comments on the manuscript. We are grateful to C.K. Shih for sending us unpublished results of his work, and for useful discussions. This work was supported by the Swiss National Science Foundation (Grant No. 20-39528.93). The computations were performed in part at ETH-CSCS (Centro Svizzero di Calcolo Scientifico). Partial support by a supercomputing grant at Cineca (Bologna, Italy) through the Istituto Nazionale di Fisica della Materia (INFM) is also acknowledged.

*Also at Institut Romand de Recherche Numérique en Physique des Matériaux (IRRMA), PHB Ecublens, CH-1015 Lausanne, Switzerland.

[1] B. Brandow, J. Alloys Compounds **181**, 377 (1992), and references therein.
[2] A. Fujimori and F. Minami, Phys. Rev. B **30**, 957 (1984).
[3] J. Zaanen, G. A. Sawatzky, and J. W. Allen, Phys. Rev. Lett. **55**, 418 (1985).
[4] Z. X. Shen *et al.*, Phys. Rev. B **44**, 3604 (1991).
[5] H. Kuhlenbeck *et al.*, Phys. Rev. B **43**, 1969 (1991).
[6] J. van Elp, H. Eskes, P. Kuiper, and G. A. Sawatzky, Phys. Rev. B **45**, 1612 (1992).
[7] S. Hüfner, P. Steiner, I. Sander, M. Neumann, and S. Witzel, Z. Phys. B **83**, 185 (1991).
[8] C. K. Shih (private communication).
[9] A. Svane and O. Gunnarsson, Phys. Rev. Lett. **65**, 1148 (1990).
[10] Z. Szotek, W. M. Temmerman, and H. Winter, Phys. Rev. B **47**, 4029 (1993).
[11] M. Arai and T. Fujiwara, Phys. Rev. B **51**, 1477 (1995).
[12] V. I. Anisimov, J. Zaanen, and O. K. Andersen, Phys. Rev. B **44**, 943 (1991).
[13] L. Hedin, Phys. Rev. **139**, A796 (1965).
[14] N. Hamada, M. Hwang, and A. J. Freeman, Phys. Rev. B **41**, 3620 (1990).
[15] F. Aryasetiawan, Phys. Rev. B **46**, 13 051 (1992).
[16] M. S. Hybertsen and S. G. Louie, Phys. Rev. Lett. **55**, 1418 (1985); Phys. Rev. B **34**, 5390 (1986).
[17] R. W. Godby, M. Schlüter, and L. J. Sham, Phys. Rev. Lett. **56**,

2415 (1986); Phys. Rev. B **35**, 4170 (1987); **37**, 10 159 (1988).
[18] R. Hott, Phys. Rev. B **44**, 1057 (1991).
[19] F. Aryasetiawan and O. Gunnarsson, Phys. Rev. Lett. **74**, 3221 (1995).
[20] S. Massidda, A. Continenza, M. Posternak, and A. Baldereschi, Phys. Rev. Lett. **74**, 2323 (1995).
[21] F. Gygi and A. Baldereschi, Phys. Rev. Lett. **62**, 2160 (1989).
[22] L. J. Sham and W. Kohn, Phys. Rev. **145**, 561 (1966).
[23] Z. H. Levine and S. G. Louie, Phys. Rev. B **25**, 6310 (1982).
[24] S. Massidda, M. Posternak, and A. Baldereschi, Phys. Rev. B **48**, 5058 (1993).
[25] H. J. F. Jansen and A. J. Freeman, Phys. Rev. B **30**, 561 (1984).
[26] *Physics of Group IV Elements and III-V Compounds*, Zahlenwerte und Funktionen aus Naturwissenschaften und Technik, edited by K.-H. Hellwege and O. Madelung, Landolt-Börnstein, New Series, Group III, Vol. 17, Pt. a (Springer, New York, 1982).
[27] G. Strinati, H. J. Mattausch, and W. Hanke, Phys. Rev. B **25**, 2867 (1982).
[28] M. Rohlfing, P. Krüger, and J. Pollmann, Phys. Rev. Lett. **75**, 3489 (1995). We quote their results obtained with the Cd^{20+} pseudopotential.
[29] M. Cardona, M. Weinstein, and G. A. Wolff, Phys. Rev. **140**, A633 (1965).
[30] L. Ley *et al.*, Phys. Rev. B **9**, 600 (1974).
[31] N. G. Stoffel, Phys. Rev. B **28**, 3306 (1983).
[32] J. E. Jaffe and A. C. Hess, Phys. Rev. B **48**, 7903 (1993).
[33] S. Massidda, R. Resta, M. Posternak, and A. Baldereschi, Phys. Rev. B **52**, R16 977 (1995).
[34] D. Vaknin, E. Caignol, P. K. Davies, J. E. Fischer, and D. C. Johnston, and D. P. Goshorn, Phys. Rev. B **39**, 9122 (1989).
[35] B. E. F. Fender, A. J. Jacobson, and F. A. Wegwood, J. Chem. Phys. **48**, 990 (1968).
[36] A. K. Cheetham and D. A. O. Hope, Phys. Rev. B **27**, 6964 (1983).
[37] D. C. Khan and R. A. Erickson, Phys. Rev. B **1**, 2243 (1970).
[38] W. L. Roth, Phys. Rev. **110**, 1333 (1958).
[39] D. Herrmann-Ronzaud, P. Burlet, and J. Rossat-Mignod, J. Phys. C **11**, 2123 (1978).
[40] S. Hüfner, J. Osterwalder, T. Riesterer, and F. Hulliger, Solid State Commun. **52**, 793 (1984).
[41] H. A. Alperin, J. Phys. Soc. Jpn. Suppl. B **17**, 12 (1962).
[42] I. A. Drabkin, L. T. Emel'yanova, R. N. Iskenderov, and Y. M. Ksendzov, Fiz. Tverd. Tela (Leningrad) **10**, 3082 (1968) [Sov. Phys. Solid State **10**, 2428 (1969)].
[43] J. van Elp *et al.*, Phys. Rev. B **44**, 6090 (1991).
[44] Y. Tokura *et al.*, Phys. Rev. B **41**, 11 657 (1990).
[45] M. R. Norman, Phys. Rev. Lett. **64**, 1162 (1990); Phys. Rev. B **44**, 1364 (1991).
[46] In the AFM calculations, $\psi_{n,\mathbf{k}\uparrow}$ and $\psi_{n,\mathbf{k}\downarrow}$ are related to each other by a translation bringing the Ni(1) into the Ni(2) sublattice.
[47] V. I. Anisimov, P. Kuiper, and J. Nordgren, Phys. Rev. B **50**, 8257 (1994).
[48] G. A. Sawatzky and J. W. Allen, Phys. Rev. Lett. **53**, 2339 (1985).
[49] M. K. Norman and A. J. Freeman, Phys. Rev. B **33**, 8896 (1986).
[50] F. Manghi, C. Calandra, and S. Ossicini, Phys. Rev. Lett. **73**, 3129 (1994). See, in particular, their Fig. 4(b).
[51] J. Laegsgaard and A. Svane (private communication).
[52] V. I. Anisimov *et al.*, Phys. Rev. B **48**, 16 929 (1993).
[53] T. Mizokawa and A. Fujimori, Phys. Rev. B **53**, 4201 (1996).
[54] M. B. Towler *et al.*, Phys. Rev. B **50**, 5041 (1994); S. Massidda *et al.* (unpublished).